Physics Letters A 374 (2010) 2850–2855

Contents lists available at ScienceDirect

Physics Letters A

www.elsevier.com/locate/pla

Negative differential conductance and effective electron mass in highly asymmetric ballistic bilayer graphene nanoribbon

Sitangshu Bhattacharya, Santanu Mahapatra *

Nanoscale Device Research Laboratory, Centre for Electronics Design and Technology, Indian Institute of Science, Bangalore, 560 012, India

ARTICLE INFO

Article history:
Received 27 January 2010
Received in revised form 22 April 2010
Accepted 30 April 2010
Available online 6 May 2010
Communicated by R. Wu

Keywords:
Graphene nanoribbon
Negative differential conductance
Effective mass

ABSTRACT

We present a simplified theory of the effective momentum mass (EMM) and ballistic current–voltage relationship in a degenerate two-folded highly asymmetric bilayer graphene nanoribbon. With an increase in the gap, the density-of-states in the lower set of subbands increases more than that of the upper set. This results in a phenomenological population inversion of carriers, which is reflected through a net negative differential conductance (NDC). It is found that with the increase of the ribbon width, the NDC also increases. The population inversion also signatures negative values of EMM above a certain ribbon-width for the lower set of subbands, which increases in a step-like manner with the applied longitudinal static bias. The well-known result for symmetric conditions has been obtained as a special case.

The high Fermi velocity of electrons in bilayer graphene (BG) has recently found potential applications in the realm of mesoscopic devices and in certain aspects of particle physics that are achievable in table-top experiments [1]. The first principle studies [2] and tight-binding model [3] applied on BG by incorporating all important interlayer interactions show that the conduction and valance bands slightly overlap near the Fermi level. These outcomes exhibit that BG should be a semimetallic material rather than a zero band gap material. A BG can also be tuned near the Dirac-point between two degenerate conduction and valance bands. This band gap tuning can be externally controlled by applying either a transverse electric field [4] or by selective doping in the two coupled hexagonal lattices with an A'–B type stacking pair [5]. In either case, this results in a potential difference between the layers, which may be called symmetric or asymmetric, depending whether the difference is zero or non-zero respectively. For investigating two port carrier transport properties, the selective doping technique is mainly preferred, since in such cases, there is no need of a transverse electric field.

Whether the carrier transport in BG, or in any other material, is diffusive or ballistic at a certain temperature, is completely determined by the carrier's mean free path (MFP) length at that temperature. Ballistic transport is said to occur when this length becomes greater than the material dimension. Otherwise it is called diffusive transport. In the past few years, investigations on both the ballistic and diffusive transport properties of carriers in BG have been done for their possible applications in nanoelectronics, spanning from the transistors to long interconnects in ultra-small integrated systems [6–15]. Extensive analyses of Hwang and Das Sarma [16] and Kubakaddi [17] suggest that although BG has an extremely nonlinear band structure, the overlap integral can be avoided since the Coulomb potential does not play a role in the determination of the phonon matrix element. Their arguments fit well in explaining electron mobility at room temperature in BG which is about 10^5 cm^2 V^{-1} s^{-1}. Their results can also be experimentally realized [18,19].

One such transport property is the carrier effective mass which is strongly connected to carrier mobility and is known to be one of the most important physical quantities used in the analysis of semiconductor devices under different physical conditions [20]. Although there are various definitions of the effective electron mass [21], it is the effective momentum mass (EMM) that should be regarded as the basic quantity [22] for the description of the carrier transport of the conduction band electrons with arbitrary band non-parabolicity [23]. However, with increasing band non-parabolicity, the EMM becomes a function of electron energy. Under carrier degeneracy, only the electrons at the Fermi surface participate in the conduction process, and hence the investigation of the EMM corresponding to the Fermi level is of interest. It may also be noted that the Fermi energy is, in turn, determined by the carrier dispersion relation and degeneracy, and thus these two features explain the behavior of the EMM in degenerate materials.

In a BG sheet, carriers are confined in a 2D plane. A further structural confinement along the lateral direction transforms the 2D system to a 1D system resulting in BG nanoribbon (BGN). Recent fabrication method sono-chemically cuts chemically derived

* Corresponding author. Tel.: +91 80 2293 3090.
E-mail address: santanu@cedt.iisc.ernet.in (S. Mahapatra).

0375-9601/$ – see front matter
doi:10.1016/j.physleta.2010.04.078

graphene sheets [24]. This results a BGN to be of several micrometers in length having a width of 20 nm or less. However, other fabrication method involves the lifting off the BG using a scotch tape and adhering onto an oxidized silicon substrate [25]. Using the electron beam lithography, contact pads are formed by a metal liftoff process using Ti/Au as the contact metal. A second layer of lithography defines nanometer-wide channels. The BGN thus prepared, finds potential applications in the area of chip-interconnects providing a substantially lower resistance than copper wire having unity aspect ratio [12]. Further, the ballistic electron thermal conductance per unit width of graphene nano-ribbons can be smaller than those of corresponding single-walled carbon nanotubes [26] which may lead to a better thermoelectric material. In case, if the width of the BG is few nanometer, the resulting lateral carrier localization leads to the van Hove singularity condition, which generates a discrete set of energy eigenvalues. When a longitudinal static bias is applied, the Fermi energy is lowered. With the increase in the bias, a chronological crossing of the Fermi level over the discrete set of subbands takes place and singularities in the variation of the EMM are thus expected for such a case.

Nevertheless, it appears from the literature that the EMM for a highly asymmetric BGN has yet to be investigated in the presence of carrier degeneracy. In this Letter, we present a simplified theoretical formulation of the EMM and a ballistic two port current–voltage relationship in an asymmetric BGN within the framework of tight binding (TB) formalism. We also report the ballistic I–V relation which signatures a phenomenological negative differential conductance (NDC) effect by considering the incorporation of the subbands due to the splitting of both sets of conduction bands.

We start with the use of TB theory by assuming each monolayer of graphene has totally l_y zigzag chains with l_x atomic sites on each chain for an asymmetric BG sheet [8]. This leads to the electron Hamiltonian near the K point as [4,8]

$$H = \begin{pmatrix} -\Delta/2 & 0 & 0 & \pi^\dagger \\ 0 & \Delta/2 & \pi & 0 \\ 0 & \pi^\dagger & \Delta/2 & \gamma \\ \pi & 0 & \gamma & -\Delta/2 \end{pmatrix} \tag{1}$$

in which l_y and l_x are the width and length of the BG, $\Delta = \phi_1 - \phi_2$, ϕ_i's are the onsite potentials on each monolayer, π $\{= v_F\hbar(-i\frac{\partial}{\partial x} + \frac{\partial}{\partial y})\}$ is the Berry phase momentum operator [4], v_F is the Fermi velocity and γ is the interlayer coupling constant. Modeling the BG as a two-coupled hexagonal lattice with a stacking pair of A'–B type, the use of Eq. (1) and a Bloch-type eigenstates $\Psi(x, y) = (\psi_A, \psi_{B'}, \psi_{A'}, \psi_A)$, where, $\psi_i(x, y) = \phi_i(y)e^{ik_x x}$, in which, $i = A, B, A', B'$ leads to the following equations:

$$-v_F\hbar\left(\frac{\partial}{\partial y} - k_x\right)\phi_B = \left(E + \frac{\Delta}{2}\right)\phi_A \tag{2}$$

$$v_F\hbar\left(\frac{\partial}{\partial y} + k_x\right)\phi_{A'} = \left(E - \frac{\Delta}{2}\right)\phi_{B'} \tag{3}$$

$$-v_F\hbar\left(\frac{\partial}{\partial y} - k_x\right)\phi_{B'} = \left(E - \frac{\Delta}{2}\right)\phi_{A'} - \gamma\phi_B \tag{4}$$

$$v_F\hbar\left(\frac{\partial}{\partial y} + k_x\right)\phi_A = \left(E + \frac{\Delta}{2}\right)\phi_B - \gamma\phi_{A'} \tag{5}$$

in which E is the electron energy as measured from the bottom of the conduction band in a vertically upward direction. Taking the values of ϕ'_B and ϕ_A from Eqs. (3) and (2) and substituting them in Eqs. (4) and (5) respectively, results in

$$\left[\left(k_x^2 - \frac{\partial^2}{\partial y^2}\right) - \left(\frac{E - \Delta/2}{v_F\hbar}\right)^2\right]\phi_{A'} + \gamma\frac{E - \Delta/2}{(v_F\hbar)^2}\phi_B = 0 \tag{6}$$

and

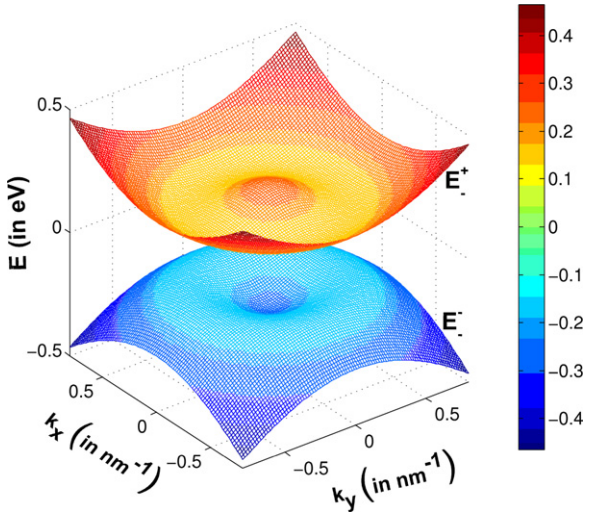

Fig. 1. Energy dispersion surface of an asymmetric BG for $\Delta = 0.25$ eV.

$$\gamma\frac{E + \Delta/2}{(v_F\hbar)^2}\phi_{A'} + \left[\left(k_x^2 - \frac{\partial^2}{\partial y^2}\right) - \left(\frac{E + \Delta/2}{v_F\hbar}\right)^2\right]\phi_B = 0 \tag{7}$$

Assuming the potentials to be constants, the solution is given by

$$\left\{k^2 - \left(\frac{E - \Delta/2}{v_F\hbar}\right)^2\right\}\left\{k^2 - \left(\frac{E + \Delta/2}{v_F\hbar}\right)^2\right\} - \gamma^2\left[\frac{E^2 - \Delta^2/4}{(v_F\hbar)^4}\right] = 0 \tag{8}$$

in which, $k^2 = k_x^2 + k_y^2$. For a symmetric case ($\Delta = \phi_1 - \phi_2 = 0$), Eq. (8) becomes

$$\left\{k^2 - \left(\frac{E}{v_F\hbar}\right)^2\right\} = \pm\gamma\frac{E}{(v_F\hbar)^2} \tag{9}$$

which at $k = 0$ converges to either $E = 0$ or $E = \pm\gamma$ for both $E > 0$ and $E < 0$ energy bands. This convergence is in accordance with the well-known result [27] and proves the mathematical compatibility of our theory.

For an asymmetric BGN, we invoke the van Hove singularity condition $k_y = \frac{n_y\pi}{l_y}$ for the Bloch type wavefunction along the y direction, which results in

$$\left\{k_x^2 + \left(\frac{n_y\pi}{l_y}\right)^2 - \left(\frac{E - \Delta/2}{v_F\hbar}\right)^2\right\}\left\{k_x^2 + \left(\frac{n_y\pi}{l_y}\right)^2 - \left(\frac{E + \Delta/2}{v_F\hbar}\right)^2\right\} = \gamma^2\left[\frac{E^2 - \Delta^2/4}{(v_F\hbar)^4}\right] \tag{10}$$

in which, n_y $(= 1, 2, 3, \ldots)$ are the van Hove singularity quantum numbers along the y direction respectively. It readily appears that Eqs. (8) and (10) generate two sets of degenerate subbands namely E_+^+, E_-^+, E_+^- and E_-^-. Fig. 1 exhibits the energy spectrum for an asymmetric BG considering the lower conduction (E_-^+) and higher valance band (E_-^-). The constant energy surfaces are the circles in the k_x–k_y plane. With an increase in asymmetry, the gap opens as shown in Fig. 2. For an asymmetric BGN, Eq. (10) transforms to

$$k_{x_\pm}^{\pm} = \pm\frac{1}{v_F\hbar}\left[E^2 + \frac{\Delta^2}{4} - \left(\frac{n_y\pi v_F\hbar}{l_y}\right)^2 \pm \sqrt{E^2(\gamma^2 + \Delta^2) - \frac{\gamma^2\Delta^2}{4}}\right] \tag{11}$$

Fig. 3(b) exhibits the energy subband structure of an asymmetric BGN. It appears that there is no inter-mixing of the conduction

energy subbands because of both E_+^+ and E_-^+. Also for $l_y = 5$ nm, there is a considerable opening of the gap about the zero level.

Using Eq. (3) and the spin and valley degeneracies ($g_s = g_v = 2$) [28], the density of states in an asymmetric BGN for both the upper (+) and lower (−) set of subbands can be derived as

$$N_{1D}^{\pm} = \frac{g_s g_v}{\pi\hbar v_F}\sum_{n_y=1}^{n_{ymax}}\left\{\left[E \pm \frac{E(\gamma^2+\Delta^2)/2}{\sqrt{E^2(\gamma^2+\Delta^2)-\frac{\gamma^2\Delta^2}{4}}}\right] \times\left[E^2+\frac{\Delta^2}{4}-\left(\frac{n_y\pi\hbar v_F}{l_y}\right)^2 \pm\sqrt{E^2(\gamma^2+\Delta^2)-\frac{\gamma^2\Delta^2}{4}}\right]^{-1/2} H\left(E-E_{n_y}^{\pm}\right)\right\} \quad (12)$$

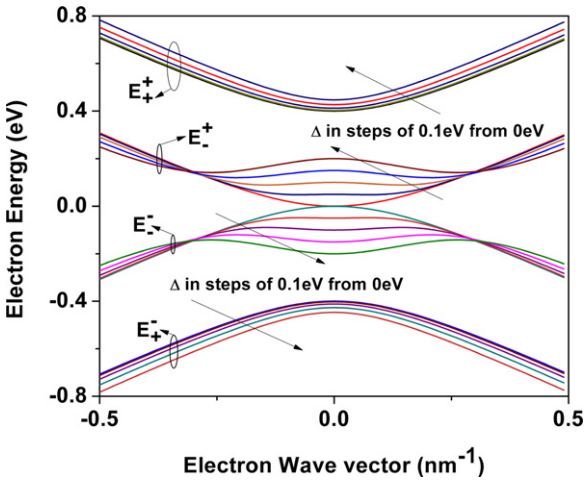

Fig. 2. E–k dispersion relation for a BG for different Δ.

in which H is the Heaviside step function and the subband energies are given by the condition $k_x^{\pm} = 0$, in which E is replaced by $E_{n_y}^{\pm}$.

For a highly asymmetric case ($\Delta = \gamma$), Eqs. (11) and (12) reduce to

$$k_x^{\pm} = \frac{1}{\hbar v_F}\left[E^2+\frac{\gamma^2}{4}-\left(\frac{n_y\pi\hbar v_F}{l_y}\right)^2 \pm\sqrt{2E^2\gamma^2-\frac{\gamma^4}{4}}\right]^{1/2} \quad (13)$$

and

$$N_{1D}^{\pm}(E) = \frac{g_s g_v}{\pi\hbar v_F}\sum_{n_y=1}^{n_{ymax}}\left[\left\{E \pm \frac{E\gamma}{\sqrt{2E^2-\frac{\gamma^2}{4}}}\right\} \times\left[E^2+\frac{\gamma^2}{4}-\left(\frac{n_y\pi\hbar v_F}{l_y}\right)^2 \pm\gamma\sqrt{2E^2-\frac{\gamma^2}{4}}\right]^{-1/2}\right] H\left(E-E_{n_y}^{\pm}\right) \quad (14)$$

Fig. 3 exhibits the energy dispersion curve of a BGN. On comparing Figs. 2 and 3, it appears that the presence of quantization along the lateral direction smoothens the bulging nature of the E_-^+ subbands. We also see from Fig. 3(b) that the presence of the van Hove singularity has a striking effect on the energy subband structure of an asymmetric BGN. This is reflected in the fact that with an increase in Δ, the lower set of subband energies starts decreasing in magnitude rather than increasing. This is directly opposite in nature to the E_-^+ conduction band as shown in Fig. 2. Also, it appears that with decreasing Δ, the energy difference between the alternate subbands of both the lower and upper set diminishes. Fig. 4 also signatures this fact. For both symmetric and asymmetric systems, the presence of γ and Δ has a profound effect on the density-of-states function in a BGN. From Fig. 4, it appears that for a symmetric BGN, states are more available in the E_+^+ rather than the E_-^+ subband; however, with the opening of the gap, states

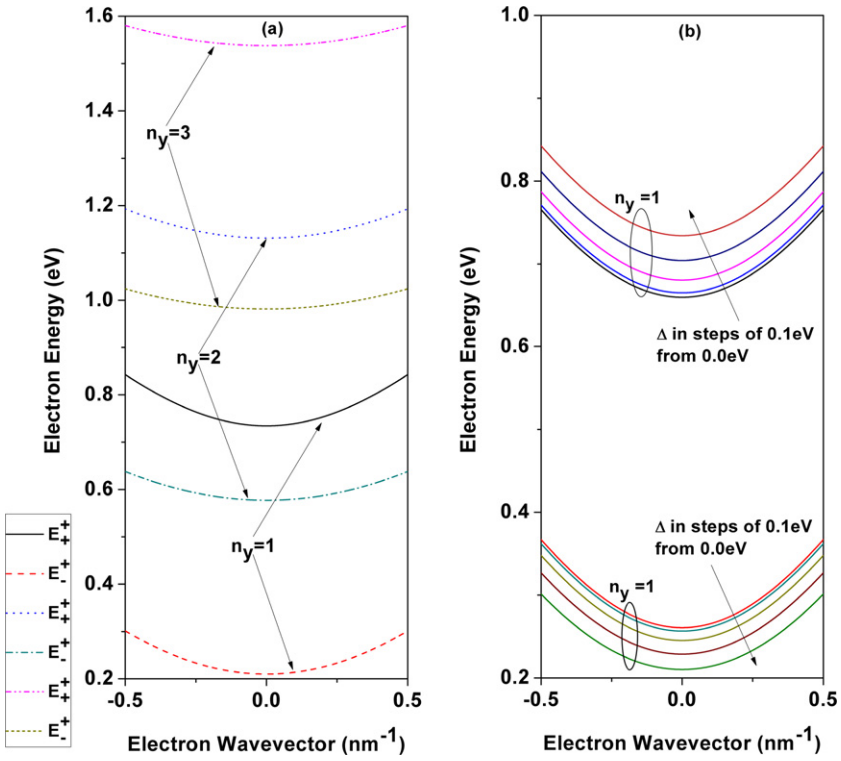

Fig. 3. Energy dispersion curves of 5 nm asymmetric BGN for (a) $\Delta = 0.4$ eV at different subbands and (b) with varying Δ for the lowest $E_+^{\pm}$ and $E_-^{\pm}$ subband.

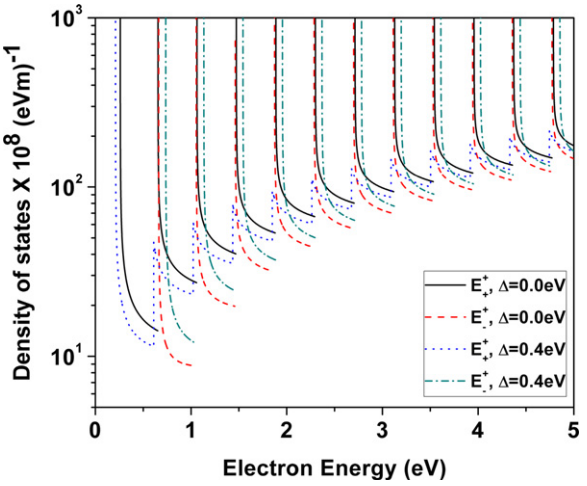

Fig. 4. Density of states as function of electron energy for 5 nm BGN at different Δ.

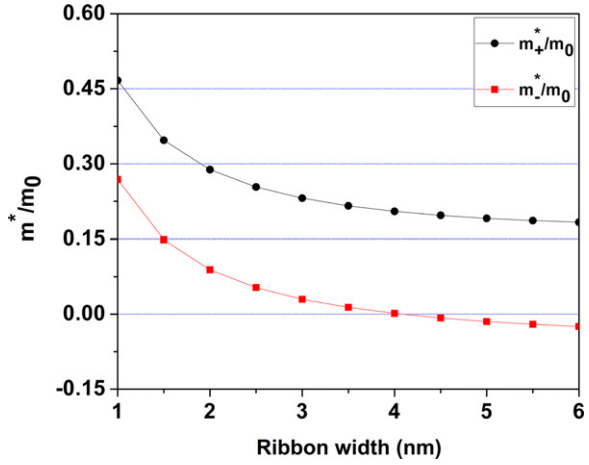

Fig. 5. Plot of the EMM for highly asymmetric BGN versus lateral width having $n_{1D} = 10^8$ m^{-1} at $T = 300$ K.

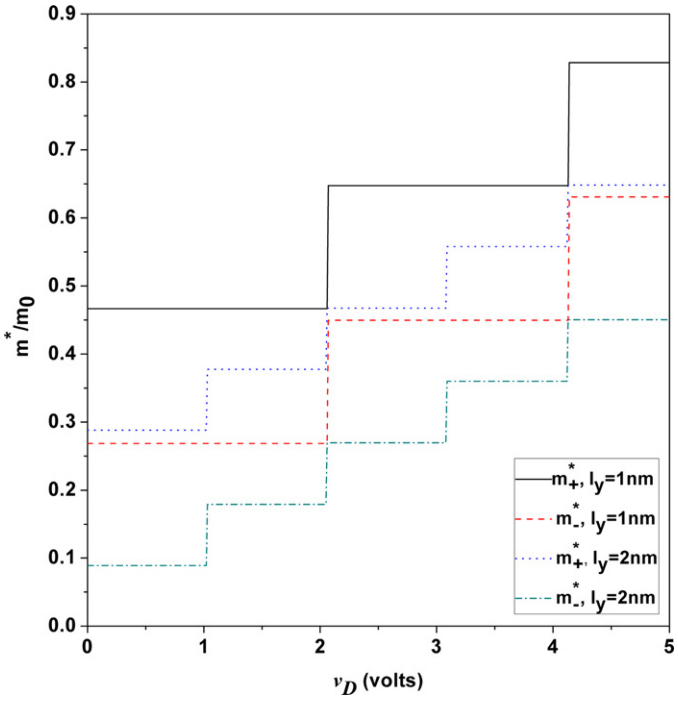

Fig. 6. Plot of the EMM for BGN versus drain bias for $n_{1D} = 10^8$ m^{-1} at $T = 300$ K.

in the E_-^+ subband increase. In this Letter, we report this phenomenological population inversion in an asymmetric BGN, which may find remarkable applications in the area of optical electronics and NDC systems.

From Fig. 2, we see that in BG, a change in Δ does not appreciably change the magnitude of E_+^+ subband energies at $k = 0$ as compared to that of E_-^+ energies. However, a lateral confinement for e.g., of 5 nm, opens a gap of about 0.2 eV about the 0 energy line at $k = 0$. It may be noted that due to the presence of two conduction bands in a BG, an extremely large transmission coefficient for a highly asymmetric diffusive BGN might be achieved when the carriers are transferred from the source to the drain. This is due to the splitting of both the conduction energy bands into a number of subbands.

Using Eq. (14), the carrier concentration can for this present case be written as

$$n_{1D} = \int_{E_{n_y}^+}^{\infty} N_{1D}^+(E) f(E)\, dE + \int_{E_{n_y}^-}^{\infty} N_{1D}^-(E) f(E)\, dE \tag{15}$$

where $f(E)$ is the Fermi–Dirac occupation probability factor. The bottom of the subband energies for the highly asymmetric case are $E_{n_y}^{\pm} = \frac{1}{2^{1/2}}[\varsigma(n_y) \pm \sqrt{\varsigma^2(n_y) - 4\xi(n_y)}]^{1/2}$, $\varsigma(n_y) = \frac{3\gamma^2}{2} + 2(\frac{n_y\pi\hbar v_F}{l_y})^2$ and $\xi(n_y) = \frac{5\gamma^4}{16} - \frac{\gamma^2}{2}(\frac{n_y\pi\hbar v_F}{l_y})^2 + (\frac{n_y\pi\hbar v_F}{l_y})^4$.

Eq. (15) results in

$$n_{1D} = n_{1D}^+ + n_{1D}^- \tag{16}$$

in which, $n_{1D}^{\pm} = \frac{g_s g_v k_B T}{2\pi\hbar v_F} \sum_{n_y=1}^{n_{y\max}} [F_0(\eta^{\pm}) - a_{\pm}\ln(1 + \frac{E_F}{E_{n_y}^{\pm}}) - \frac{b_{\pm}(n_y)}{k_B T} \times (\frac{E_F - E_{n_y}^{\pm}}{E_F E_{n_y}^{\pm}}) + \frac{c_{\pm}(n_y)}{k_B T}(\frac{E_F^2 - (E_{n_y}^{\pm})^2}{E_F^2 (E_{n_y}^{\pm})^2}) - \frac{d_{\pm}}{k_B T}(\frac{E_F^3 - (E_{n_y}^{\pm})^3}{E_F^3 (E_{n_y}^{\pm})^3}) - \frac{e(n_y)}{k_B T}(\frac{E_F^4 - (E_{n_y}^{\pm})^4}{E_F^4 (E_{n_y}^{\pm})^4})]$, $\eta^{\pm} = \frac{1}{k_B T}[E_F - E_{n_y}^{\pm}]$, $a^{\pm} = (1 \mp 1)$, $b_{\pm}(n_y) = \frac{1}{2}(\pm\gamma^2 + \theta^2(n_y))$, $\theta^2(n_y) = \{\gamma^2 - (\frac{n_y\pi\hbar v_F}{l_y})^2\}$, $c_{\pm}(n_y) = \frac{1}{2}\{\pm\sqrt{2} + \frac{1\mp 1}{\sqrt{2}}\}\gamma\theta^2(n_y)$, $d_{\pm}(n_y) = \frac{1}{2}\{\pm(1 \mp 1) + \frac{1}{2}\}\gamma^2\theta^2(n_y)$, $e(n_y) = \sqrt{2}\frac{\gamma^3}{4}\theta^2(n_y)$, and $F_j(\eta)$ is the one parameter Fermi–Dirac integral of order j [29] and E_F is the Fermi energy. The EMM in general can be written as [22,23]

$$m_{\pm}^*(E_F) = \hbar^2 k \frac{\partial k}{\partial E}\bigg|_{E=E_F} \tag{17}$$

Using Eqs. (13) and (17), the EMM in a highly asymmetrical ($\Delta = \gamma$) BGN along the longitudinal direction can be derived as

$$m_{\pm}^*(E_F) = \frac{E_F}{v_F^2}\left[1 \pm \frac{2\gamma}{\sqrt{2E_F^2 - \frac{\gamma^2}{4}}}\right] \tag{18}$$

However, for a symmetric case,

$$m_{\pm}^*(E_F) = \frac{E_F}{v_F^2}\left[1 \pm \frac{\gamma}{E_F}\right] \tag{19}$$

Eq. (19) exhibits the fact that the EMM in lower subband can become negative if $E_F < \gamma$, where, $\gamma = 0.4$ eV [27]. This has been exhibited in Fig. 5. For a heavily doped symmetric BGN, $E_F \gg \gamma$ and in such a case, the EMM in both the subbands approaches $m^*(E_F) = 0.176 E_F m_0$, where, m_0 is the free electron mass. The variation of the EMM as a function of ribbon-width has been shown in Fig. 5. Fig. 6 exhibits the variation of the EMM as a function of drain bias. With an increase in the ribbon or well width, the Fermi energy is reduced, and this, in turn, reduces the EMM in both the lower and upper set of subbands. Moreover, the EMM for an asymmetric BGN can become larger than that of the asymmet-

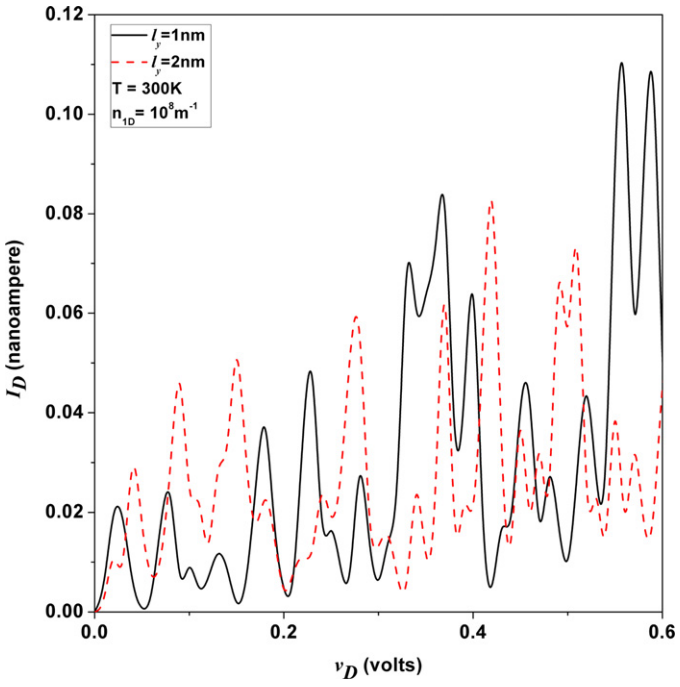

Fig. 7. Plot of the negative differential conductance in BGN for $n_{1D} = 10^8$ m^{-1} at $T = 300$ K.

ric BG, which is also a direct signature of quantum confinement. The rates at which the EMM decrease are determined by the constants of the energy spectra of graphene. As one increases drain bias, step dependencies are expected due to the crossing over of the Fermi level by size-quantized levels. For each coincidence of a size quantized level with the Fermi level, there is a discontinuity in the density-of-states function resulting in a quantum jump. The appearance of humps in the curves of Fig. 6 is due to the redistribution of the electrons among the quantized energy levels when the size quantum number corresponding to the highest occupied level changes from one fixed value to another. With large ribbon-width, the height of the steps decreases and the EMM approaches its BG value. It appears that the carriers in the lower set of subbands possess a lower EMM. Hence, when in the diffusive regime, the contributions to electron mobility in BGN can mainly be due to them. For $\Delta = 0$, m_-^{*+} exhibits negative values until $E_F = \gamma$. In such a case, $m_-^{*+} = 0$ and $m_+^{*+} = 2\gamma/v_F^2 \sim 0.411 m_0$. The physical reason behind the lower mass m_-^{*+} is because of the increase in the available states (or population inversion) in the lower subband band due to the opening of the gap.

The current law for an 1D ballistic system for the present case using Natori's model [30] can be written as

$$I_D = \frac{g_s g_v e}{h} \sum_{n_y=1}^{n_{ymax}} \int_{E_{n_y}^{\pm}}^{\infty} \left[\left\{ 1 + \exp\left[\frac{E - (E_F + e v_D)}{k_B T} \right] \right\}^{-1} - \left\{ 1 + \exp\left[\frac{E - E_F}{k_B T} \right] \right\}^{-1} \right] dE \tag{20}$$

which simplifies to

$$I_D = \frac{g_s g_v e k_B T}{h} \sum_{n_y=1}^{n_{ymax}} \left[F_0(\eta_{\pm}^R) - F_0(\eta_{\pm}^L) \right] \tag{21}$$

where, $\eta_{\pm}^R = \frac{1}{k_B T}[E_F + e v_D - E_{n_y}^{\pm}]$ and $\eta_{\pm}^L = \frac{1}{k_B T}[E_F - E_{n_y}^{\pm}]$. Using Eqs. (16), (21) and allied equations, Fig. 7 exhibits the current–voltage characteristics of a highly asymmetric BGN. The direct signature of population inversion is exhibited in Fig. 7, where we see that NDC occurs when the drain voltage is increased. With the increase in the lateral width, the drain current increases. When the temperature is high enough, the first two terms in the equation of $n_{1D}^{\pm}$ dominate; however, as the temperature tends to zero, all the rest of the other terms dominate in the determination of the carrier Fermi energy. It may be noted that the dual peaks in Fig. 7 are due to the singularities governed by Eq. (16) for the two sets of subbands.

At this point, we note that we have not considered the many body effects in this simplified theoretical formalism. Our simplified approach will be useful for the purpose of comparison when methods of tackling the formidable problem after inclusion of these effects for the present systems appear. The inclusion of the said effects would certainly increase the accuracy of the results, although the qualitative features of the EMMs and the current–voltage characteristics in a highly asymmetric BGN as discussed in this Letter will not change in the presence of the aforementioned effects.

The variation in the EMMs and the NDC effect in the current–voltage characteristics as presented in this Letter reflect a direct signature of the application of an asymmetrically biased BGN in optical and transferred electron devices, where resistances can be controlled by opening the gap. The theoretical results as given here would be useful in analyzing various other experimental data related to this phenomenon. Finally, we can state with conviction that this theory can be used to investigate the effective electron mass, and other different diffusive transport coefficients of an asymmetric BGN operated under the influence of an external photon field.

Acknowledgements

This work was supported by Department of Science and Technology (DST), India under Grant No. SR/FTP/ETA-37/08.

References

[1] A.H.C. Neto, F. Guinea, N.M.R. Peres, K.S. Novoselov, A.K. Geim, Rev. Mod. Phys. 81 (2009) 109.
[2] S. Latil, L. Henrard, Phys. Rev. Lett. 97 (2006) 036803(1).
[3] Y.H. Lai, J.H. Ho, C.P. Chang, M.F. Lin, Phys. Rev. B 77 (2008) 085426(1).
[4] E.V. Castro, K.S. Novoselov, S.V. Morozov, N.M.R. Peres, J.M.B. Lopes dos Santos, J. Nilsson, F. Guinea, A.K. Geim, A.H.C. Neto, Phys. Rev. Lett. 99 (2007) 216802(1).
[5] T. Ohta, A. Bostwick, T. Seyller, K. Horn, E. Rotenberg, Science 313 (2006) 951.
[6] I. Snyman, C.W.J. Beenakker, Phys. Rev. B 75 (2007) 045322(1).
[7] J. Cserti, Phys. Rev. B 75 (2007) 033405(1).
[8] R. Ma, L.J. Zhu, L. Sheng, M. Liu, D.N. Sheng, Europhys. Lett. 87 (2009) 17009(1).
[9] M.I. Katsnelson, Eur. Phys. J. B 52 (2006) 151.
[10] Q. Shao, G. Liu, D. Teweldebrhan, A.A. Balandin, S. Rumyantsev, M.S. Shur, D. Yan, IEEE Electron Device Lett. 30 (2009) 288.
[11] A. Naeemi, J.D. Meindl, IEEE Electron Device Lett. 28 (2007) 428.
[12] A. Naeemi, J.D. Meindl, IEEE Trans. Electron Devices 56 (2009) 1822.
[13] M. Barbier, P. Vasilopoulos, F.M. Peeters, J.M. Pereira Jr., Phys. Rev. B 79 (2009) 155402(1).
[14] M. Koshino, T. Ando, Phys. Rev. B 73 (2006) 245403(1).
[15] B. Sahu, H. Min, A.H. MacDonald, S.K. Banerjee, Phys. Rev. B 78 (2008) 045404(1).
[16] E.H. Hwang, S. Das Sarma, Phys. Rev. B 77 (2008) 115449(1).
[17] S.S. Kubakaddi, Phys. Rev. B 79 (2008) 075417(1).
[18] K.S. Novoselov, A.K. Geim, S.V. Morozov, D. Jiang, Y. Zhang, S.V. Dubonos, I.V. Grigorieva, A.A. Firsov, Science 306 (2004) 666.
[19] Y.B. Zhang, Y.W. Tan, H.L. Stormer, P. Kim, Nature 438 (2005) 201.
[20] S. Adachi, J. Appl. Phys. 58 (1985) R1.
[21] R. Dornhaus, G. Nimtz, Springer Tracts in Modern Physics, Springer, Berlin, 1976.
[22] W. Zawadzki, in: W. Paul (Ed.), Handbook of Semiconductor Physics, vol. 1, North-Holland Publishing Company, Amsterdam, 1982, pp. 713–720.
[23] I.M. Tsidilkovski, Band Structures of Semiconductors, Pergamon Press, London, 1982.

[24] Z.-S. Wu, W. Ren, L. Gao, B. Liu, J. Zhao, H.-M. Cheng, Nano Res. 3 (2010) 16.
[25] R. Murali, K. Brenner, Y. Yang, T. Beck, J.D. Meindl, IEEE Electron Device Lett. 30 (2009) 611.
[26] E. Watanabe, S. Yamaguchi, J. Nakamura, A. Natori, Phys. Rev. B 80 (2009) 085404(1).
[27] A. Das, B. Chakraborty, S. Piscanec, S. Pisana, A.K. Sood, A.C. Ferrari, Phys. Rev. B 79 (2009) 155417(1).
[28] B.E. Feldman, J. Martin, A. Yacoby, Nature Phys. Lett. 5 (2009) 889.
[29] J.S. Blakemore, Semiconductors Statistics, Dover Publications, New York, 1987.
[30] K. Natori, J. Appl. Phys. 76 (1994) 4879.